



CHORUS

This is the accepted manuscript made available via CHORUS. The article has been published as:

Tungsten Hexanitride with Single-Bonded Armchairlike Hexazine Structure at High Pressure

Nilesh P. Salke, Kang Xia, Suyu Fu, Youjun Zhang, Eran Greenberg, Vitali B. Prakapenka, Jin Liu, Jian Sun, and Jung-Fu Lin

Phys. Rev. Lett. **126**, 065702 — Published 8 February 2021

DOI: [10.1103/PhysRevLett.126.065702](https://doi.org/10.1103/PhysRevLett.126.065702)

Tungsten hexanitride with single-bonded armchair-like hexazine structure at high pressure

Nilesh P. Salke^{1,#,*}, Kang Xia^{2,3}, Suyu Fu⁴, Youjun Zhang⁵, Eran Greenberg⁶, Vitali B. Prakapenka⁶, Jin Liu^{1,*}, Jian Sun^{2,*}, Jung-Fu Lin^{4,*}

¹ Center for High Pressure Science and Technology Advanced Research, Beijing 100094, China

² National Laboratory of Solid State Microstructures, School of Physics and Collaborative Innovation Center of Advanced Microstructures, Nanjing University, Nanjing, 210093, P. R. China

³ Department of Applied Physics, College of Science, Nanjing Forestry University, Nanjing, 210037, P. R. China

⁴ Department of Geological Sciences, Jackson School of Geosciences, The University of Texas at Austin, Austin, TX 78712, USA

⁵ Institute of Atomic and Molecular Physics, Sichuan University, Chengdu, 610065, China

⁶ Center for Advanced Radiation Sources, University of Chicago, Chicago, IL 60637, USA

Corresponding Authors Email:

* afu@jsg.utexas.edu (JFL)

* jiansun@nju.edu.cn (JS)

* jin.liu@hpstar.ac.cn (JL)

* nilesh@uic.edu (NPS)

Current Affiliation: Department of Physics, University of Illinois at Chicago, Chicago, 60607, USA

Abstract

WN₆ has been discovered at 126-165 GPa after heating of W in nitrogen. XRD refinements reveal a unit cell in space group $R\bar{3}m$ which is consistent with the WN₆ structure with armchair-like hexazine (N₆) rings, while strong A_{1g} Raman mode confirms its polymeric N-N single bonds. DFT calculations reveal balanced contributions of attractive interactions between W and covalent N₆ rings and repulsions between N₆ rings that make WN₆ ultra stiff and tough. The WN₆ displays long bond lengths in nearest N-N and pressure-enhanced electronic band gap, which pave the way for finding novel nitrides.

Main Text

Diatomic nitrogen is the most abundant molecule of the Earth's atmosphere accounting for almost 78% by volume. The strong triple bond in nitrogen ($\text{N}\equiv\text{N}$) makes it highly stable and unreactive at near ambient conditions. At high pressure-temperature (P-T) conditions, nitrogen can form double or even single-bonded solids ($\text{N}=\text{N}$, $\text{N}-\text{N}$).¹ Of particular interest is to find single-bonded nitrogen with a huge difference in the average bond energy: transformation of a single bonded polymeric nitrogen into a triple bonded nitrogen molecule is expected to accompany a tremendous energy release.² Thus far, searching for single-bonded nitrogen has gained tremendous research interest because of its unique physical properties and potentials in high energy density (HED) materials. Previous theoretical predictions and experiments have showed that a number of single-bonded nitrogen allotropes can exist at ultrahigh P or P-T conditions.^{1, 3-9} Key observations in past studies include the cubic gauche nitrogen (cg-N) synthesised at ~ 110 GPa and ~ 2000 K in a diamond anvil cell (DAC)⁷, the layered polymeric nitrogen (LP) with *Pba2* structure⁵ at ~ 125 GPa, and the hexagonal layered polymeric nitrogen (HLP-N) with tetragonal *P4₂bc* structure at ~ 250 GPa after laser heating¹. Very recently, black phosphorus structured nitrogen (bp-N) has also been found at 140 GPa by laser heating.^{3, 4} Particularly, the HLP-N consists of distorted and interconnected hexagonal N_6 rings with N-N single bonds in its structure. Its discovery has renewed the interest of finding the sought-after yet hypothetical planar hexazine N_6 ring of nitrogen argued to be thermodynamically unstable due to the strong lone pair repulsion.^{10, 11}

Nitrogen-bearing compounds has been suggested to a promising means to search for polymeric N_6 ring at high P-T.¹²⁻¹⁶ Recently, transition metal nitrides (TMNs) have drawn much attention for their exceptional physical properties such as high melting point, chemical inertness, high incompressibility and hardness.¹⁷ Similar to nitrogen, nitrogen-rich nitrides with single and double nitrogen bonds have also gathered much attention due to their HED application.¹⁸⁻²⁴ Recent theoretical calculations have predicted the occurrence of transition metal hexanitrides at high P-T including WN_6 , TeN_6 , MoN_6 and ReN_6 .¹²⁻¹⁶ These hexanitrides are predicted to be stable in an $R\bar{3}m$ structure which contains armchair-like N_6 rings with single bonds between adjacent nitrogen atoms. Tungsten hexanitrides (WN_6) stands out in particular because of its high melting point and thermal stability as well as ultrahigh Vickers hardness of ~ 57 GPa, the highest among TMNs.¹³ WN_6 also possesses unique features of ionic-like crystals and an enlarged band gap with compression¹³, which is opposite to normal semiconductors such as silicon. Nitrogen-rich WN_6 has very good gravimetric and volumetric

energy density, making it a potential HED material. Interestingly, WN_6 is predicted to be metastable even at ambient pressure so it is possible to recover.^{12, 13} However, the thermodynamic stability pressure for WN_6 predicted by different theoretical models varies significantly from 16 GPa¹² to 65 GPa¹³. This highlights the degree of difficulty to accurately predict the stability and structure of polynitride in correlated transition metals. Most importantly, to the best of our knowledge, the hexazine-bearing TMN has not been synthesized experimentally up to now so its physical and chemical properties remain unknown experimentally.

High P-T conditions are useful to overcome the energy barrier and synthesize new TMN phases. Inspired by a recent theoretical study¹³, here we have carried out high P-T DAC experiments coupled with *in-situ* X-ray diffraction (XRD) measurements up to 165 GPa and 3500 K to explore new chemical compounds in the W-N system. We have successfully synthesized and refined the novel WN_6 phase in the $R\bar{3}m$ structure at 126-165 GPa after heating. Together with high-pressure Raman spectroscopy measurements and theoretical predictions, our results show that the WN_6 contains armchair-like hexazine (N_6) rings with strong covalent N-N single bonds stabilized by balanced attractive-repulsive interactions within crystal. These experimental results are used to benchmark new first-principles calculations which further demonstrate ultrahigh hardness and toughness of WN_6 .

Three independent XRD experiments in pulsed laser-heated DACs were carried on tungsten samples loaded with ultrapure nitrogen at high P-T at 13IDD beamline, GSECARS, Advanced Photon Source (See Figures S2, S3 and S4 and detailed description in Supplemental Material²⁵). XRD analysis of the initially loaded tungsten samples showed them to be stable in body-centered cubic (*bcc*) structure at high pressure without laser heating. After initial laser heating of the W samples surrounded by nitrogen at approximately 114 GPa, new diffraction peaks were observed and can be indexed as $\text{WN}_8 \cdot \text{N}_2$ phase which was previously reported³⁷ (Figures S3, S4 and S6 in Supplemental Material²⁵). In addition, cg-N phase observed⁷ (Figures S3 and S4 in Supplemental Material²⁵). Upon further heating up to 3500 K at ~126 GPa, additionally many new diffraction peaks appeared (Figure S3 in Supplemental Material²⁵) and these peaks could be indexed to a rhombohedral crystal class with lattice parameters $a = 5.6786(5) \text{ \AA}$, $c = 4.2057(4) \text{ \AA}$, $V = 117.45(5) \text{ \AA}^3$. With further compression and heating cycles up to the maximum experimental pressure of 165 GPa, diffraction peaks became stronger and all peaks except those corresponding to unreacted W can be well indexed to the rhombohedral phase signalling the stability of the new WN_6 at higher pressures (Figure 1a). Le Bail

refinements of the diffraction patterns at 165 GPa confirm that these new peaks correspond to a new phase with the $R\bar{3}m$ structure having lattice parameters of $a = 5.591(1)$ Å and $c = 4.145(1)$ Å (Figure 1a). The refined space group and lattice parameters are in excellent agreement with the theoretically predicted WN_6 phase with the $R\bar{3}m$ structure^{12, 13} at 165 GPa with lattice parameters, $a = 5.596$ Å and $c = 4.144$ Å. In the $R\bar{3}m$ structured WN_6 , nitrogen atoms form novel armchair N_6 rings and tungsten atoms sit midway in-between two N_6 rings along the c crystallographic axis (Figure 1b)¹³. Further, during the decompression cycles, the diffraction peaks for the WN_6 phase could be found to pressures as low as 68 GPa, before the unfortunate breaking of one of the diamonds. cg-N and $WN_8 \cdot N_2$ phases also co-existed with WN_6 up to 152 GPa in compression and up to 68 GPa in decompression cycle (Figure S3 in Supplemental Material²⁵). In brief recount, our experimental results show the occurrence of the $R\bar{3}m$ -structured WN_6 at pressures between 126 and 165 GPa after laser heating (Figure S7 in Supplemental Material²⁵).

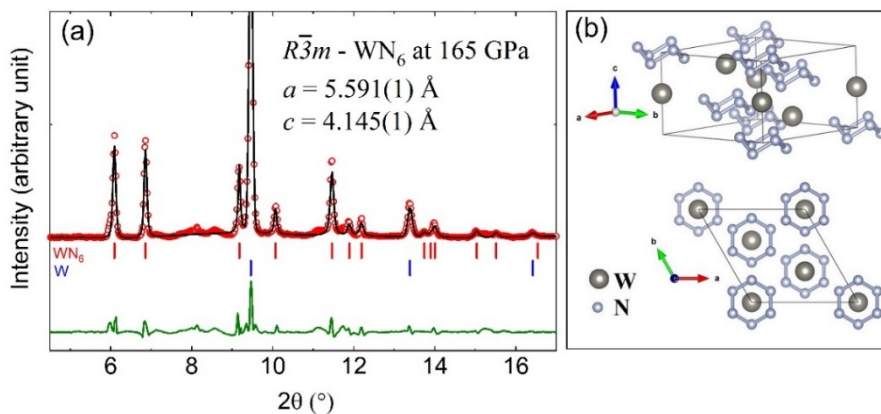


Figure 1: Crystal structure of WN_6 with the space group $R\bar{3}m$ determined by high-pressure XRD refinement. (a) Le Bail refinement of WN_6 at 165 GPa ($\lambda = 0.3344$ Å) (red vertical ticks). W (blue vertical ticks) represents unreacted W in the bcc phase that co-exists with the WN_6 . (b) Crystal structure of WN_6 with the novel armchair N_6 rings and W atoms in-between the rings along c axis.¹³ See a representative XRD image at 165 GPa shown in Figure S5 in Supplemental Material²⁵.

High-pressure micro-Raman measurements³⁸ of the laser-heated areas for WN_6 and theoretical predictions on vibrational modes at Γ point were performed to better understand the nature of the N_6 rings and vibrational symmetries in the WN_6 . Raman spectra of the WN_6 recorded at 165 GPa display intense peaks at around 760, 905 and 1057 cm^{-1} (Figure 2a). Factor group analysis for possible vibrational modes in $R\bar{3}m$ structured WN_6 shows that 21 zone centre vibrational phonon modes can be assigned as $\Gamma = 2A_{1g} + A_{1u} + A_{2g} + 3A_{2u} + 3E_g + 4E_u$. Out of these, a total of five different ($2A_{1g} + 3E_g$) Raman active modes are expected in 400-

1600 cm^{-1} wavenumber range (Figure 2a). These theoretically calculated modes (red vertical ticks in Figure 2a) are generally in good agreement with the experimental peak positions. Direct comparison between theory and experiments indicates that the vibrational mode around 1057 cm^{-1} arises from A_{1g} symmetry, while both 760 and 905 cm^{-1} vibrations are assigned to be of E_g symmetry. The agreement here leads us to use the Eigen vectors for the experimentally observed Raman modes to illustrate the magnitude and direction of the nitrogen atomic displacements in the N_6 ring (red arrows in Figure 2b). All three Eigen vectors represent the coupled motions for the opposite nitrogen atoms in N_6 ring, that are characteristic of the armchair-like single-bonded N_6 vibrations. Particularly, the symmetric stretching motions of opposite nitrogen atoms viewing from the top view of the N_6 ring contribute to the characteristic Raman peaks at 1057 cm^{-1} of the A_{1g} symmetry. Our experimental observation and theoretical predictions of the high-wavenumber A_{1g} vibration mode at 1057 cm^{-1} confirm the single-bonding character between adjacent nitrogen atoms in the N_6 rings of WN_6 (Figs. 1-2). The observation of this high-wavenumber Raman peak is consistent with experimentally-observed Raman shift range in other single bonded polymeric nitrogen phases such as cg-N and bp-N: all these phases display the vibrational modes around 800 to 1300 cm^{-1} range at megabar pressure region corresponding to single-bonded nitrogen vibrations (Figure S8 in Supplemental Material²⁵).^{3-5, 7}

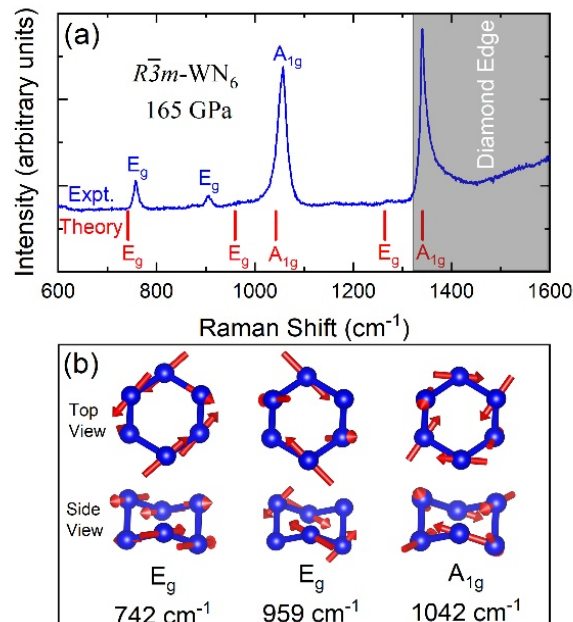


Figure 2: Representative Raman spectrum and Eigen vectors of the $R\bar{3}m$ structured WN_6 at high pressure. (a) Raman spectrum of WN_6 recorded at 165 GPa (excitation wavelength, $\lambda = 532$ nm). The red vertical ticks represent the positions of theoretical Raman-active modes of WN_6 . Based on the comparison with theory,

experimentally observed peaks are assigned vibrational symmetries labelled next to the peaks. (b) Eigen vectors for three experimentally observed modes. Symmetries and theoretically calculated equivalent Raman shifts are also labelled for clarity. The red arrows indicate the direction and magnitude of nitrogen atomic displacements in the N_6 rings, as viewed from the top and the side.

Pressure-dependent unit cell parameters, d-spacings, and volume of WN_6 are obtained from refinements of the XRD spectra in the pressure range of 68 to 165 GPa (Figures 3 and S9). Using third-order Birch-Murnaghan equation of state (EOS) to fit the experimental data, axial incompressibility of the WN_6 are 338(8) GPa for a -axis and 324(10) GPa for c -axis, respectively, which mean that the pressure dependence of the c/a ratio is nearly constant within uncertainties (Figure 3a). The EOS parameters for WN_6 are $B_0 = 329(8)$ GPa with $B_0' = 4$ fixed and $V_0 = 49.6(2)$ $\text{\AA}^3/\text{f.u.}$ B_0 is found to be in good agreement with a theoretically predicted value of 302.7 GPa¹³, supporting the highly incompressible nature of WN_6 . We have performed new theoretical calculations on lattice and EOS parameters by PBE and PBE-D3 functionals, and the results are consistent with these experimental parameters (Figures 3a and 3b). The high-pressure EOS curve calculated by PBE functional (violet dashed line in Figure 3c agrees with the experimental and fitting results at low pressures (≤ 90 GPa). With continued compression, the PBE results exhibit an increasing difference of larger volume compared to the experimental values. This may originate from the ignoring weak non-covalent interactions between the quasi-molecular N_6 rings, which could shrink the cell at high pressures. Based on a previous report, each covalent-bonded N_6 ring obtains around 2.4e Bader charge.¹³ Similar order of the charge transfer is also found in the N_6 rings of TeN_6 .¹⁵ These motivate us to investigate the weak non-covalent interactions between N_6 rings. After taking weak non-covalent interactions into account by employing the DFT-D3 dispersion correction method in the revised PBE-D3 functional,^{39,40} the predicted lattice parameters and volume are found to be in better agreement with the experimental data especially in the pressure range of 120–170 GPa, as the blue dashed line shows as in Figure 3. These results highlight the rhombohedral unit cell of WN_6 is extremely stiff yet experiences almost isotropic compression that reflects the balanced contributions of the strong covalent nitrogen rings, the attractive ionic interactions between W and N_6 rings, and the repulsive interactions between the N_6 rings. (Figure 1b, 3b).

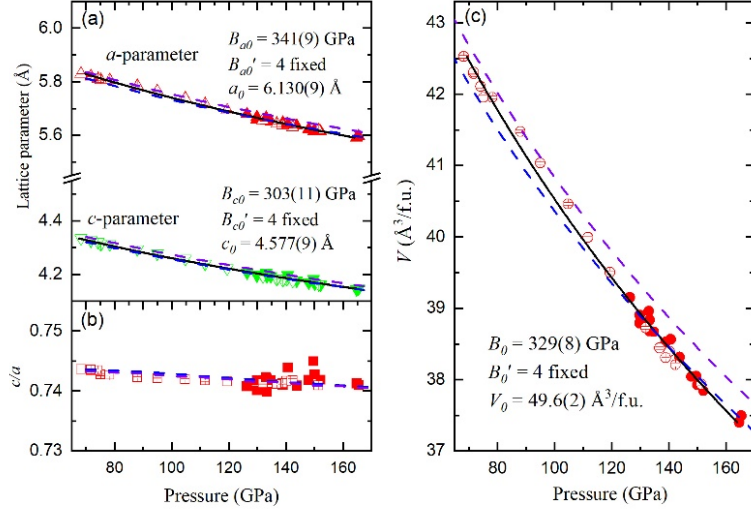


Figure 3: Unit cell parameters and volume of the $R\bar{3}m$ structured WN_6 at high pressure. (a) Pressure-dependent unit cell parameters of WN_6 , from XRD results. Solid and open red triangles represent a -parameter in compression and decompression cycle respectively. Solid and open green triangles represent c -parameter in compression and decompression cycle respectively. Black continuous lines represent fitting of the axial incompressibility using 3rd B-M EOS. Violet and blue dash lines represent the calculated EOS by PBE and PBE-D3 functional. (b) Pressure dependence of experimental c/a ratio compared with calculated c/a . Red solid and open squares are experimental data for compression and decompression cycle respectively. Violet and blue dash lines represent data calculated by PBE and PBE-D3 functional respectively. (c) Pressure-dependent unit cell volume of WN_6 fitted by 3rd B-M EOS. Solid and open red circles represent volume in compression and decompression cycle respectively and black line represents experimental EOS. Experimental EOS compared with the theoretical results using plain PBE (violet dashed line) and PBE-D3 (blue dashed line) functionals.

Further, the EOS parameters of WN_6 are compared with other single-bonded polymeric nitrogen phases (Table S1 in Supplemental Material²⁵) to help understand the behaviour of single-bonded nitrogen sublattices at high pressure. The incompressibility of the N-sublattice in WN_6 is 341(13) GPa, which is relatively higher than that in cg-N ($B_0 = 298(6)$ GPa)⁷ and bp-N ($B_0 = 183$ GPa)⁴, but is comparable with that in HLP-N ($B_0 = 349(40)$ GPa)¹. This observation indicates that the N_6 structural unit is very stiff and plays an essential role in the ultrahigh incompressibility of the WN_6 unit cell. To better understand the effect of weak non-covalent interactions between the N_6 rings on the lattice and EOS parameters, we have further performed calculations using charge density-based methods. Weak non-covalent interactions were observed directly by calculating two- and three-dimensional reduced density gradient (Figure S10 in Supplemental Material²⁵). The non-covalent interactions (NCIs) such as the attractive interactions between W atoms and N_6 rings and repulsive interactions between the N_6 rings coexist in WN_6 . Coexistence of these interaction compensates each other to stabilize armchair-like hexazine ring in WN_6 at high pressures and contribute to its ultrahigh

incompressibility. Furthermore, the calculated nearest N-N bond length in WN_6 is 1.46 Å at ambient pressure and 1.39 Å at 130 GPa. Among the known polymeric nitrogen phases, HLP-N also consists of distorted N_6 ring structure, however this phase is only found to be stable above 240 GPa. The nearest N-N bond length of HLP-N is 1.30 Å at 235 GPa¹, whereas it is 1.31 Å at 400 GPa in WN_6 . By comparison, the nearest bond length for single-bonded nitrogen atoms is 1.346(4) Å in cg-N at 115 GPa⁷, and is 1.338(6) Å in bp-N at 140 GPa³. Notably, N-N bond length in the range ~1.30 - 1.46 Å corresponds to high incompressibility. Interestingly, WN_6 is found to have the longest N-N bond length between nearest nitrogen atoms (N-N) among different TMNs (Figure 4a). That is, other nitrogen-rich nitrides with single-bonded nitrogen and long nearest N-N bond lengths could also be highly incompressible.

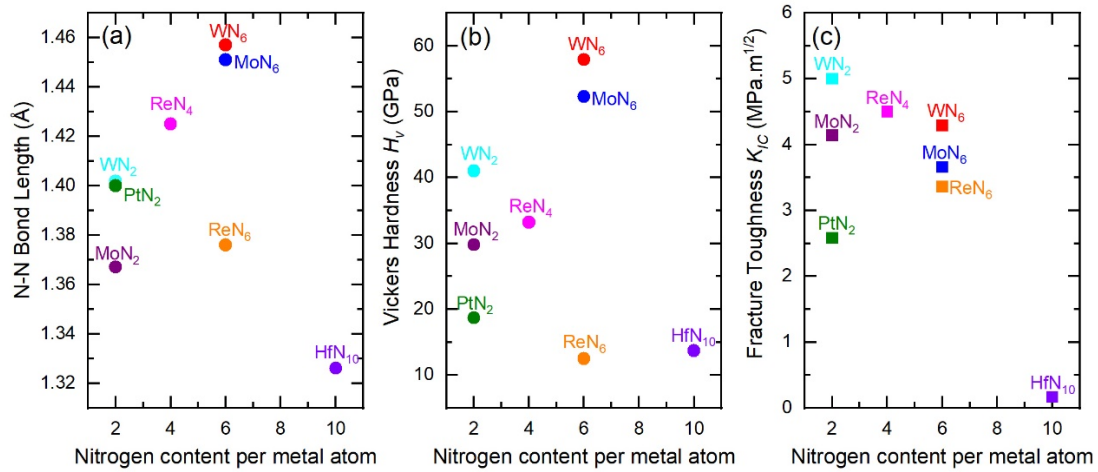


Figure 4: Comparisons of the bond length, hardness and toughness of WN_6 with other nitrogen compounds. (a) Theoretically calculated nearest N-N bond length for representative nitrides with nitrogen content (x) per metal atom. [References: WN_6 ¹³, MoN_6 ¹⁴, ReN_6 ¹⁴, *P4/mbm* WN_2 ⁴¹ and MoN_2 ⁴², *Cmmm* ReN_4 ⁴³, *Immm* HfN_{10} ⁴⁴ and pyrite-type PtN_2 ⁴⁵] (b) The theoretically calculated Vickers hardness (H_v , GPa) for different nitrides with nitrogen content (x) per metal atom. The hardest known transition metal (M) nitrides (MN_x) are compared. (c) The calculated fracture toughness (K_{IC} , $\text{MPa}\cdot\text{m}^{1/2}$) for different nitrides with nitrogen content (x) per metal atom. Several MN_x with high toughness are selected for comparison.

In order to better understand the mechanical properties of WN_6 , full elastic constants (C_{ij} 's) of WN_6 are also calculated at ambient pressure (Table S2 in Supplemental Material²⁵). The bulk modulus (B) and shear modulus (G) of WN_6 at ambient pressure are calculated from the C_{ij} 's and its density, which are 302.7 and 315.7 GPa, respectively (Table S3 in Supplemental Material²⁵). For detailed comparison, the C_{ij} and mechanical modulus (B and G) from previously reported nitrides with different nitrogen content are listed in Tables S2 and S3, respectively, See Supplemental Material²⁵, including the isostructural MoN_6 and ReN_6 ,¹⁴

$P4/mbm$ WN_2 ⁴¹ and MoN_2 ,⁴² $Cmmm$ ReN_4 ,⁴³ $Immm$ HfN_{10} ,⁴⁴ and pyrite-type PtN_2 ⁴⁵. As shown in Table S3 in Supplemental Material²⁵, the $R\bar{3}m$ -structured WN_6 has the highest G among the known transition metal nitrides. Based on the widely used semi-empirical models by Chen *et al.*⁴⁶ and Tian *et al.*⁴⁷, we estimated the Vickers hardness H_v of all the interesting transition metal nitrides. The WN_6 is found to be superhard and possesses the highest Vickers hardness (57.9 GPa) among the nitrides (Figure 4b). Nearest N-N bond length is showing nearly consistent relation with hardness of TMNs (Figures 4a and 4b). Fracture toughness (K_{IC}) for different nitrides calculated using empirical model by Niu *et al.*⁴⁸ (Figure 4c and Table S3 in Supplemental Material²⁵). With G of 315.7 GPa and a low Pugh modulus ratio B/G of 0.96, the WN_6 can reach a high K_{IC} of around 4.29 $MPa \cdot m^{1/2}$. This value is slightly below that of WN_2 and ReN_4 but can be considered high because materials with high hardness usually tend to have low K_{IC} values. Our calculations here indicate that WN_6 has a good balance between superhardness and fracture toughness, which is important for applications. Based on theoretical calculations¹³, the superhardness of the WN_6 can be attributed to the electron repulsion between W and N atoms that helps to open the electronic band gap and result in the non-metallicity in WN_6 .

In summary, we have successfully synthesised the $R\bar{3}m$ structured WN_6 at 126-165 GPa after laser heating to as high as $\sim 3,500$ K. The WN_6 contains novel armchair-like N_6 rings that are manifested in the E_g and A_{1g} Raman active modes at 760, 905, and 1057 cm^{-1} . The refined lattice parameters, and Raman active modes of WN_6 are in excellent agreement with theoretical calculations. The strong covalent N-N single bonds in N_6 ring, the ionic interactions between the N_6 rings and the tungsten atoms and repulsive electrostatic interaction between N_6 rings are the main attributes of the ultrahigh incompressibility of the WN_6 . The armchair-like hexazine nitrogen sublattice in the WN_6 is remarkably comparable to that in the polymeric nitrogen phases and can be a high-energy density material candidate. Calculations of the elastic moduli indicate that the WN_6 exhibits superhardness and good fracture toughness. Future efforts in the synthesis and recovery of TMNs will lead to a wealth of knowledge in the novel chemistry and physical properties of the single-bonded hexazine-bearing nitrides.

ACKNOWLEDGMENTS

N.P.S. acknowledges the postdoc fellowship support at the Center for High Pressure Science and Advanced Technology Research (HPSTAR). J.S. gratefully acknowledges financial support from the National Key R&D Program of China (Grant No. 2016YFA0300404), the

National Natural Science Foundation of China (Grant Nos. 11974162 and 11834006), the Fundamental Research Funds for the Central Universities. K.X. acknowledges the financial support from the Project funded by China Postdoctoral Science Foundation (Grant No. 2019M651767). Y.Z. acknowledge support from the National Natural Science Foundation of China (No. 11872077). The numerical calculations in this paper were performed on the computing facilities in the High Performance Computing Center of Collaborative Innovation Center of Advanced Microstructures, the High Performance Computing Center (HPCC) of Nanjing University and “Tianhe-2” at NSCC-Guangzhou. XRD experiments were conducted at GeoSoilEnviroCARS of Advanced Photon Source (APS), Argonne National Laboratory (ANL). GeoSoilEnviroCARS operations are supported by the National Science Foundation-Earth Sciences (EAR-1634415) and the Department of Energy, Geosciences (DE-FG02-94ER14466). Part of this research used resources of the Advanced Photon Source, a U.S. Department of Energy (DOE) Office of Science User Facility operated for the DOE Office of Science by Argonne National Laboratory under Contract No. DE AC02-06CH11357.

References

1. D. Laniel, G. Geneste, G. Weck, M. Mezouar and P. Loubeyre, *Physical Review Letters* **122** (6), 066001 (2019).
2. M. J. Greschner, M. Zhang, A. Majumdar, H. Liu, F. Peng, J. S. Tse and Y. Yao, *The Journal of Physical Chemistry A* **120** (18), 2920-2925 (2016).
3. D. Laniel, B. Winkler, T. Fedotenko, A. Pakhomova, S. Chariton, V. Milman, V. Prakapenka, L. Dubrovinsky and N. Dubrovinskaia, *Phys Rev Lett* **124** (21), 216001 (2020).
4. C. Ji, A. A. Adeleke, L. Yang, B. Wan, H. Gou, Y. Yao, B. Li, Y. Meng, J. S. Smith, V. B. Prakapenka, W. Liu, G. Shen, W. L. Mao and H. K. Mao, *Sci Adv* **6** (23), eaba9206 (2020).
5. D. Tomasino, M. Kim, J. Smith and C.-S. Yoo, *Physical Review Letters* **113** (20), 205502 (2014).
6. M. J. Lipp, J. P. Klepeis, B. J. Baer, H. Cynn, W. J. Evans, V. Iota and C. S. Yoo, *Physical Review B* **76** (1), 014113 (2007).
7. M. I. Eremets, A. G. Gavriliuk, I. A. Trojan, D. A. Dzivenko and R. Boehler, *Nature Materials* **3** (8), 558-563 (2004).
8. C. J. Pickard and R. J. Needs, *Physical Review Letters* **102** (12), 125702 (2009).
9. A. K. McMahan and R. LeSar, *Physical Review Letters* **54** (17), 1929-1932 (1985).
10. T.-K. Ha, R. Cimiraglia and M. T. Nguyen, *Chemical Physics Letters* **83** (2), 317-319 (1981).
11. H. Huber, *Angewandte Chemie International Edition in English* **21** (1), 64-65 (1982).
12. Q. Li, L. Sha, C. Zhu and Y. Yao, *EPL (Europhysics Letters)* **118** (4), 46001 (2017).
13. K. Xia, H. Gao, C. Liu, J. Yuan, J. Sun, H.-T. Wang and D. Xing, *Science Bulletin* **63** (13), 817-824 (2018).
14. Q. Wei, C. Zhao, M. Zhang, H. Yan and B. Wei, *Physics Letters A* **383** (20), 2429-2435 (2019).
15. Z. Liu, D. Li, Q. Zhuang, F. Tian, D. Duan, F. Li and T. Cui, *Communications Chemistry* **3** (1), 42 (2020).
16. C. Lu and C. Chen, *Physical Review Materials* **4** (4), 043402 (2020).
17. V. L. Solozhenko and E. Gregoryanz, *Materials Today* **8** (11), 44-51 (2005).
18. C. Zhang, C. Sun, B. Hu, C. Yu and M. Lu, *Science* **355** (6323), 374-376 (2017).

19. B. A. Steele, E. Stavrou, J. C. Crowhurst, J. M. Zaug, V. B. Prakapenka and I. I. Oleynik, *Chemistry of Materials* **29** (2), 735-741 (2017).
20. S. Wei, D. Li, Z. Liu, X. Li, F. Tian, D. Duan, B. Liu and T. Cui, *Physical Chemistry Chemical Physics* **19** (13), 9246-9252 (2017).
21. D. Laniel, G. Weck, G. Gaiffe, G. Garbarino and P. Loubeyre, *The Journal of Physical Chemistry Letters* **9** (7), 1600-1604 (2018).
22. Z. Liu, D. Li, S. Wei, Y. Liu, F. Tian, D. Duan and T. Cui, *Physics Letters A* **383** (28), 125859 (2019).
23. Z. Liu, D. Li, Y. Liu, T. Cui, F. Tian and D. Duan, *Physical Chemistry Chemical Physics* **21** (22), 12029-12035 (2019).
24. K. Xia, X. Zheng, J. Yuan, C. Liu, H. Gao, Q. Wu and J. Sun, *The Journal of Physical Chemistry C* **123** (16), 10205-10211 (2019).
25. See Supplemental Material at [link] for experimental and theoretical calculations details, Tables S1–S3, Figures S1–S10 and bibliography, which includes references [26–36].
26. W. Humphrey, A. Dalke and K. Schulten, *Journal of Molecular Graphics* **14** (1), 33-38 (1996).
27. G. Kresse and J. Furthmüller, *Physical Review B* **54** (16), 11169-11186 (1996).
28. J. P. Perdew, K. Burke and M. Ernzerhof, *Physical Review Letters* **77** (18), 3865-3868 (1996).
29. G. Shen, M. L. Rivers, Y. Wang and S. R. Sutton, *Review of Scientific Instruments* **72** (2), 1273-1282 (2001).
30. V. B. Prakapenka, A. Kubo, A. Kuznetsov, A. Laskin, O. Shkurikhin, P. Dera, M. L. Rivers and S. R. Sutton, *High Pressure Research* **28** (3), 225-235 (2008).
31. A. Otero-de-la-Roza, M. A. Blanco, A. M. Pendás and V. Luaña, *Computer Physics Communications* **180** (1), 157-166 (2009).
32. E. R. Johnson, S. Keinan, P. Mori-Sánchez, J. Contreras-García, A. J. Cohen and W. Yang, *Journal of the American Chemical Society* **132** (18), 6498-6506 (2010).
33. K. Momma and F. Izumi, *Journal of Applied Crystallography* **44** (6), 1272-1276 (2011).
34. A. Otero-de-la-Roza, E. R. Johnson and V. Luaña, *Computer Physics Communications* **185** (3), 1007-1018 (2014).
35. C. Prescher and V. B. Prakapenka, *High Pressure Research* **35** (3), 223-230 (2015).
36. A. Togo and I. Tanaka, *Scripta Materialia* **108**, 1-5 (2015).
37. M. Bykov, S. Chariton, E. Bykova, S. Khandarkhaeva, T. Fedotenko, A. V. Ponomareva, J. Tidholm, F. Tasnadi, I. A. Abrikosov, P. Sedmak, V. Prakapenka, M. Hanfland, H. P. Liermann, M. Mahmood, A. F. Goncharov, N. Dubrovinskaia and L. Dubrovinsky, *Angew Chem Int Ed Engl* **59** (26), 10321-10326 (2020).
38. N. Holtgrewe, E. Greenberg, C. Prescher, V. B. Prakapenka and A. F. Goncharov, *High Pressure Research* **39** (3), 457-470 (2019).
39. S. Grimme, S. Ehrlich and L. Goerigk, *Journal of Computational Chemistry* **32** (7), 1456-1465 (2011).
40. S. Grimme, J. Antony, S. Ehrlich and H. Krieg, *The Journal of Chemical Physics* **132** (15), 154104 (2010).
41. H. Yan, M. Zhang, Q. Wei and P. Guo, *Journal of Alloys and Compounds* **581**, 508-514 (2013).
42. S. Yu, B. Huang, X. Jia, Q. Zeng, A. R. Oganov, L. Zhang and G. Frapper, *The Journal of Physical Chemistry C* **120** (20), 11060-11067 (2016).
43. Z. Zhao, K. Bao, D. Li, D. Duan, F. Tian, X. Jin, C. Chen, X. Huang, B. Liu and T. Cui, *Scientific Reports* **4** (1), 4797 (2014).
44. J. Zhang, A. R. Oganov, X. Li and H. Niu, *Physical Review B* **95** (2), 020103 (2017).
45. J. C. Crowhurst, A. F. Goncharov, B. Sadigh, C. L. Evans, P. G. Morrall, J. L. Ferreira and A. J. Nelson, *Science* **311** (5765), 1275 (2006).
46. X.-Q. Chen, H. Niu, D. Li and Y. Li, *Intermetallics* **19** (9), 1275-1281 (2011).
47. Y. Tian, B. Xu and Z. Zhao, *International Journal of Refractory Metals and Hard Materials* **33**, 93-106 (2012).
48. H. Niu, S. Niu and A. R. Oganov, *Journal of Applied Physics* **125** (6), 065105 (2019).

